Defect Removal in the Course of Directed Self-Assembly is Facilitated in the Vicinity of the Order-Disorder Transition

Weihua Li, Paul F. Nealey, Juan J. de Pablo, and Marcus Müller

Phys. Rev. Lett. **113**, 168301 — Published 15 October 2014

DOI: 10.1103/PhysRevLett.113.168301

Defect removal in the course of directed self-assembly is facilitated in the vicinity of the order-disorder transition

Weihua Li,[1,2] Paul F. Nealey,[3,4] Juan J. de Pablo,[3,4] and Marcus Müller[1*]
[1] *Institute for Theoretical Physics, Georg-August University, 37077 Göttingen, Germany*
[2] *State Key Laboratory of Molecular Engineering of Polymers, Department of Macromolecular Science, Fudan University, Shanghai 200433, China*
[3] *Institute for Molecular Engineering, University of Chicago, IL 60637 USA and*
[4] *Argonne National Laboratory, Argonne, IL 60439, USA*

The stability of prototypical defect morphologies in thin films of symmetric diblock copolymers on chemically patterned substrates is investigated by self-consistent field theory. The excess free energy of defects and barriers of defect-removal mechanisms are obtained by computing the minimum free-energy path. Distinct defect-removal mechanisms are illustrated demonstrating that (i) defects will become unstable at a characteristic value of incompatibility, χN_*, *above* the order-disorder transition and (ii) the kinetics is accelerated at weak segregation. Numerical findings are placed in the context of physical mechanisms and implications for directed self-assembly are discussed.

The self-assembly of block copolymers has attracted abiding interest because it provides a platform for fabricating dense, ordered structures at the nanoscale [1–6]. Block copolymer lithography aims to enable high-resolution and high-throughput patterning at low cost by combining the advantages of traditional lithographic techniques with the self-assembly of block copolymers on the length scale of $5 - 70$ nm [7, 8]. Practical applications often require morphologies with extremely small defect densities and precise control of orientation and alignment. This can be achieved by directing the self-assembly of copolymer materials by topographically structured (graphoepitaxy [9–12]) or chemically patterned (chemoepitaxy [13–16]) substrates.

Defects, however, are experimentally observed in directed self-assembly (DSA) [17] although their free energy, ΔF_d, exceeds the thermal energy, $k_\mathrm{B}T$, by two orders of magnitude [12, 18]. Thus, experimentally observed defects cannot be conceived as rare equilibrium fluctuations of an aligned morphology. Instead, they are created in the course of structure formation. Understanding the kinetics of DSA one can tailor the process conditions to avoid formation of defects in the early stages of DSA or to accelerate their annihilation [19].

In this Letter we focus on lamella-forming copolymers on substrate patterns of lines and spaces and explore metastability and removal mechanisms of prototypical dislocation or jog defects. We relate our observations to basic physical mechanisms that may also provide guiding principles for more complex defects.

We consider an incompressible melt of symmetric AB diblock copolymers confined between a neutral top surface and a bottom substrate with a chemical guiding pattern of A- and B-attractive stripes. The incompatibility between blocks is characterized by the product, χN, of Flory-Huggins parameter, χ and number of segments, N. Volume, film thickness, mean-squared end-to-end distance of the copolymers, and bulk lamellar period are denoted by V, D, $R_{\mathrm{e}0}$, and L_0, respectively. We choose $D = 0.8L_0$, frustrating parallel lamellae. The system contains 5 stripes of length $16L_0/3$. It is comprised of n copolymer molecules, and the invariant degree of polymerization is $\sqrt{\mathcal{N}} = nR_{\mathrm{e}0}{}^3/V$. Confining surfaces in the xy plane are modeled by reflecting boundaries. The substrate interaction is represented by $H_\mathrm{sub}(\mathbf{r}) = -\Lambda_0 k_\mathrm{B}T R_{\mathrm{e}0}{}^3\psi(x)\delta(z)$ with $\psi(x) = \pm 1$ characterizing the lateral stripe pattern with periodicity, $L_\mathrm{s} = L_0$. Λ_0 quantifies the strength of interaction between segments and guiding pattern. The substrate free energy of a perfectly aligned morphology is $\gamma_\mathrm{sub}R_{\mathrm{e}0}{}^2/k_\mathrm{B}T\sqrt{\mathcal{N}} = -\Lambda_0 N$. $R_{\mathrm{e}0}$, χN, $\sqrt{\mathcal{N}}$, and $\Lambda_0 N$ do not depend on the definition of a segment.

The free energy of a morphology is calculated within self-consistent field theory [20, 21]. Rather than describing a morphology by the spatially varying composition, we use the thermodynamically conjugated variable, the exchange chemical potential $W(\mathbf{r})$, as order parameter [12, 22]. The improved string method [23] is employed to compute the minimum free energy path (MFEP) of the free-energy functional, $F[W]$. The MFEP estimates the most probable defect-removal path; fluctuations around this path are ignored. This path is a string of morphologies, $W_\alpha(\mathbf{r})$, parameterized by a contour variable, $0 \le \alpha \le 1$ and defined by the condition that the gradient of the free energy perpendicular to the MFEP vanishes. The starting morphology, $W_0(\mathbf{r})$ corresponds to a defect, whereas the ending morphology, $W_1(\mathbf{r})$, represents the aligned, defect-free lamellar state. The MFEP of $F[W]$ has successfully been used to identify saddle points of morphological transitions in block copolymer systems [12, 22]. Minima and saddle points of $F[W]$ coincide with those of the free-energy functional of the local composition difference. Details of the path may, however,

*Corresponding author. E-mail: mmueller@theorie.physik.uni-goettingen.de

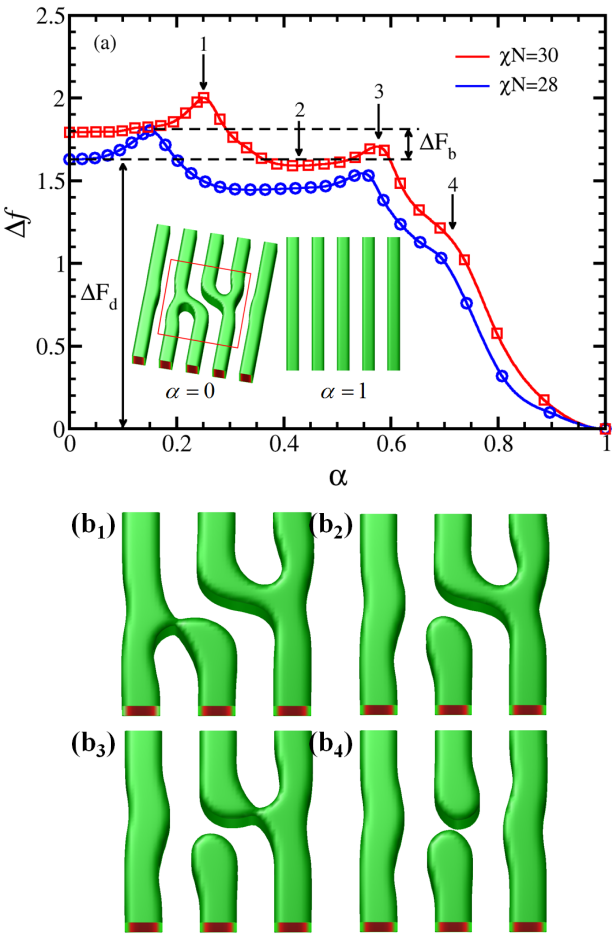

Figure 1: (a) Minimum free-energy path (*2D-MFEP*) between defect, $\alpha = 0$, and lamellar structure, $\alpha = 1$, without guiding pattern. The dimensionless free energy difference, $\Delta f = R_{e0}\Delta F_b/Dk_BT\sqrt{N}$, per film thickness as a function of the contour parameter, α, along the *2D-MFEP* is shown. The excess free energy, ΔF_d, and the highest barrier, ΔF_b, are indicated for incompatibilities $\chi N = 28$ and 30. Additional, characteristic stages along the *2D-MFEP* are indicated by the numbered arrows, and the corresponding intermediate morphologies (iso-surfaces of A density of the central portion indicated by the red box in the morphology, $\alpha = 0$, of panel (a)) are shown in panels (b_1) $\alpha \approx 0.250$, (b_2) $\alpha \approx 0.428$, (b_3) $\alpha \approx 0.577$, and (b_4) $\alpha \approx 0.710$.

depend on the choice of the order parameter and local conservation laws [24].

Quasi-2D mechanism – First we consider defect removal on a substrate in the absence of a guiding pattern, $\Lambda_0 N = 0$. Top surface and bottom substrate are identical and both ends of the MFEP – defect and perfect lamellae – are translationally invariant in z direction, i.e. two-dimensional. Thus, one could expect that all morphologies along the MFEP are also two-dimensional. If we initialize the MFEP from a dislocation-dipole defect to a defect-free lamellar structure with strictly two-dimensional morphologies, indeed, even in three-dimensional calculations such a MFEP of two-dimensional morphologies will remain stable.

This *2D-MFEP*, presented in Fig. 1 a, shows that both, the excess free energy, ΔF_d, of the defect as well as the highest barrier, ΔF_b, along the MFEP, increase with incompatibility. For both values of χN, the morphologies along the MFEP, characterizing the defect-removal mechanism, are qualitatively similar. The removal of a B-core dislocation-dipole is triggered by breaking one connection between two A-domains (see panel b_1, $\alpha \approx 0.250$). This topological change of morphology has the highest free-energy barrier and, according to Kramers' theory, the corresponding Boltzmann factor, $\exp(\Delta F_b/k_BT)$, dictates the defect-removal rate. The free-energy barrier, ΔF_b, is about an order of magnitude smaller than the excess free energy, ΔF_d, of the defect. Subsequently, the morphology relaxes into a metastable minimum, $\alpha \approx 0.428$ see Fig. 1 b_2. Further along the *2D-MFEP*, this metastable edge dislocation is annihilated by breaking the remaining A connection. The saddle-point morphology, $\alpha \approx 0.577$, is presented in panel b_3. This second free-energy barrier, however, is smaller than the first one and, therefore, it is not the rate-limiting step. There is an additional shoulder, $\alpha \approx 0.71$, in the free-energy profile, which is associated with the fusion of the two disconnected A-lamellae (cf. Fig. 1 b_4). The absence of a barrier demonstrates that this morphology with two, apposing end-caps of A-domains is even not metastable.

The strategy of breaking A connections sequentially, instead of simultaneously, and forming an intermediate edge-dislocation defect reduces the dominant free-energy barrier. Takahashi *et al.* [12] have also observed a similar sequential mechanism with multiple barriers in two-dimensional calculation connecting a dislocation defect and a defect-free lamellar structure in graphoepitaxy.

Wetting-like mechanism – The propensity of block copolymer systems to form localized defects gives rise to a rugged free-energy landscape [25], in which there may be multiple MFEPs connecting the same two morphologies. It is a challenge to identify the MFEP with the smallest barrier. In the following, we explore one alternative defect-removal mechanism exploiting that the morphology along the MFEP may vary along the z direction. Fig. 2 presents this *MFEP2* on a patterned substrate, $\Lambda_0 N = 0.11$, and unpatterned substrate, $\Lambda_0 N = 0$.

MFEP2 for $\Lambda_0 N = 0.11$ also involves a sequence of two saddle points (or one saddle point and a shoulder), which are associated with the sequential breaking of the two A connections. In contrast to the *2D-MFEP*, the morphology of the first saddle point, depicted in panel b_1, shows that the connection is first broken at the bottom substrate. The saddle point corresponds to a wedge-shaped A domain where the two internal AB interfaces touch each other at the substrate whereas the connection is still of width $L_0/2$ at the top surface.

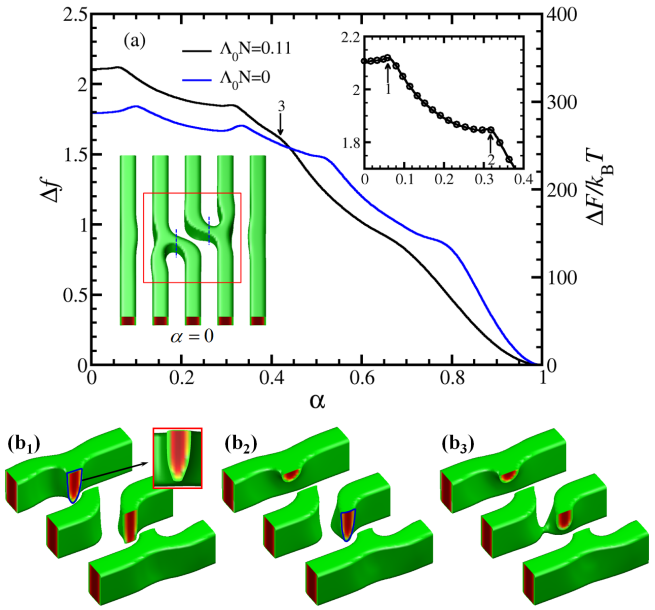

Figure 2: (a) *MFEP2* for $\chi N = 30$ and $\Lambda_0 N = 0$ and 0.11. The inset enlarges the region near the barrier for $\Lambda_0 N = 0.11$. The alternate ordinate shows the absolute free energy for $\sqrt{\bar{\mathcal{N}}} = 128$. ($b_1$), ($b_2$), and ($b_3$): three intermediate morphologies for $\Lambda_0 N = 0.11$ located at the barrier, $\alpha \approx 0.059$, and the two shoulders, $\alpha \approx 0.318$ and $\alpha \approx 0.420$, respectively. The morphology has been twice cleaved along an xz plane (indicated by the blue lines in the morphology of panel (a)) to show the cross-section of the A connections.

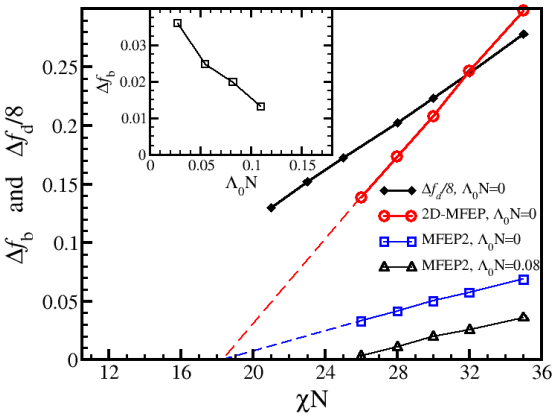

Figure 3: Defect free energy, $\Delta f_{\rm d} = R_{\rm e0}\Delta F_{\rm d}/Dk_{\rm B}T\sqrt{\bar{\mathcal{N}}}$ (scaled by 1/8), and free-energy barrier, $\Delta f_{\rm b} = R_{\rm e0}\Delta F_{\rm b}/Dk_{\rm B}T\sqrt{\bar{\mathcal{N}}}$, for different mechanisms as a function of χN. The inset presents the dependence of $\Delta f_{\rm b}$ of *MFEP2* on $\Lambda_0 N$ at $\chi N = 30$.

Once the connection is broken at the bottom guiding pattern, a continuous B domain is formed on the B-preferential stripe. The local morphology at the substrate replicates the guiding pattern, whereas there remains an A domain at the top surface. These two domains are separated by an AB interface parallel to the substrate. This parallel AB interface moves upwards away from the guiding pattern, i.e., the thickness of the aligned B lamella growths whereas the thickness of the misaligned A connection at the top surfaces shrinks. This thickening of the B lamella, which is preferred by the guiding pattern, can be conceived as the wetting of the aligned grain [26] in analogy to what has been observed in studies of the kinetics of structure formation [17]. Therefore, we characterize the complex, three-dimensional defect morphology along this portion of *MFEP2* by a single reaction coordinate – the perpendicular position, h, of the interface between the aligned B lamella at the substrate and the misaligned A connection at the top.

Before this A connection vanishes, $h \approx 0.7D$, the *MFEP2* exhibits a shoulder or small barrier (cf. panel b_2) that signals the breaking of the second A connection and the formation of an aligned B domain at the patterned substrate. The thickness of this aligned B domain also increases with α. The subsequent shoulder marks the formation of an A connection on the central A-attractive stripe that starts the fusion of the dis-connected A lamellae (see panel b_3). The final shoulder in the free-energy profiles corresponds to the elimination of the thin, misaligned grain from the film, $h \to D$. As we reduce the strength, $\Lambda_0 N$, of the guiding pattern to zero, *MFEP2* remains distinct from *2D-MFEP* (cf. Figs 1 and 2) illustrating the possibility of multiple paths with different symmetries.

In Fig. 3 we explore the dependence of the defect free energy and free-energy barrier on incompatibility, χN. In the range, $21 \le \chi N \le 32$, $\Delta F_{\rm d}$ and $\Delta F_{\rm b}$ vary approximately linear with χN. The free-energy barrier, $\Delta F_{\rm b}$, extrapolates to 0 around $\chi N_* > \chi N_{\rm ODT} \approx 10.5$, distinctly above the order-disorder transition (ODT). In marked contrast, the excess free energy of the defects, $\Delta F_{\rm d}$, remains large and finite at χN_*. *Thus, there is an interval around χN_*, where defects are not even metastable, $\Delta F_b \ll k_{\rm B}T$, and spontaneously convert into defect-free lamellae, yet the defect free energy is large, $\Delta F_d \gg k_{\rm B}T$, such that defects do not form by thermal fluctuations. It is this interval where we expect that DSA results in rapid, defect-free self-assembly.*

This observation is one of the multiple reasons why solvent [27–30] or thermal [31] annealing, which reduces the incompatibility, facilitates defect-free ordering.

The observation that the barrier of *2D-MFEP* vanishes before the ODT is also compatible with the two-dimensional studies of graphoepitaxy [12]. The alternate mechanism, *MFEP2*, however, has the lower free-energy barrier. Intriguingly, the barriers of these two distinct pathways on unpatterned substrates, $\Lambda_0 N = 0$, appear both to vanish at a similar incompatibility, $\chi N_* \approx 18$. This observation may indicate an intrinsic property of

the copolymer morphology. We speculate that the loss of metastability is associated with interactions between the distorted internal AB interfaces of the defect that provide the thermodynamic driving force for defect removal. In the weak segregation limit, the width, w, of the internal interfaces and the spatial range, over which deviations from the bulk lamellar structure distort the morphology, are comparable to the size of a defect, $L_0 \sim R_{e0}$, promoting topological changes of the morphology. In the strong segregation limit, however, there is a separation between the width of the internal interfaces and the lamellar period, $w/L_0 \sim 1/\sqrt{\chi N} \ll 1$. This is the first reason why defect removal is facilitated in the weak-segregation limit [32].

As we increase the strength, $\Lambda_0 N$, of the guiding pattern, χN_* increases. The defect-removal mechanism, *MFEP2*, corresponds to the formation and thickening of the aligned grain at the guiding pattern of the substrate. This can be conceived as the analog of the wetting of the aligned grain on the guiding pattern in the laterally restricted area of the defect. The metastability of the defect is associated with a barrier in the interface potential, $g(h)$, that quantifies the free-energy cost of placing the grain boundary between the aligned grain and the defect morphology a distance, h, above the patterned substrate. The vanishing of ΔF_b corresponds to the wetting spinodal. Invoking Cahn's argument [33], that there is a wetting transition upon approaching a critical point, we conclude that the aligned grain will wet the guiding pattern at $\chi N_{wet} > \chi N_{ODT}$. There are corrections to this wetting-like description of defect removal that stem from additional interactions with the finite-sized defect with the neighboring lamellae [34] but this physical interpretation captures the salient properties: the existence of an incompatibility $\chi N_{wet} \approx \chi N_* > \chi N_{ODT}$, below which defects cease to be metastable and the increase of χN_* with $\Lambda_0 N$. Thus, it provides a second reason why defect removal is facilitated in the vicinity of the ODT.

Evaporation-like mechanism – In Fig. 4 we present the MFEP from two apposing dislocations, which result in the formation of an additional B domain of length L for $\Lambda_0 N = 0$. The length L continuously shrinks and the free-energy linearly decreases with L (cf. dashed line in Fig 4); only when the additional domain vanishes, $L \to 0$, the free-energy profile exhibits a shoulder. Although there is no barrier, defect removal is protracted at large χN [35]. This intrinsic slowness [36] stems from the "evaporation" of B blocks inside the additional B domain through the A domain in order to decrease L. This "evaporation" of a B block through an A domain exposes its segments to the incompatible environment and gives rise to a barrier of order $\chi N/2$ for the *single-chain dynamics* (similar to diffusion across lamellae [37]) although there is no collective free-energy barrier in the MFEP. The field-theoretic approach that uses collective variables can include this activated process of a single chain through the

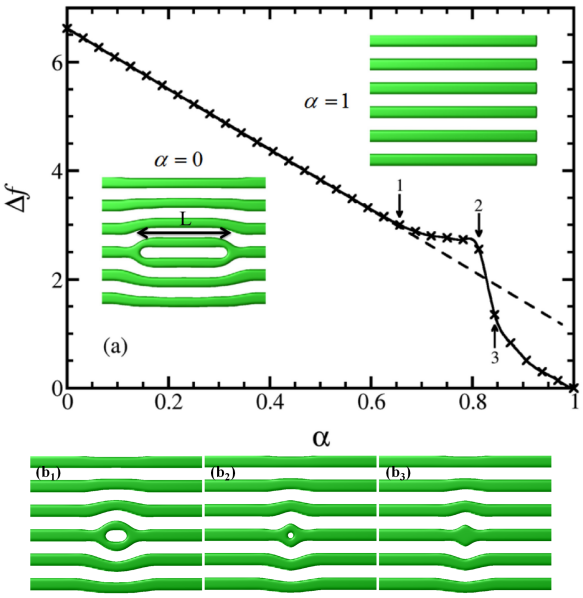

Figure 4: (a) MFEP for the removal of two apposing disclinations at $\chi N = 30$. (b_1)-(b_3): three intermediate morphologies located at $\alpha \approx 0.656$), $\alpha \approx 0.812$, and $\alpha \approx 0.844$, respectively.

Onsager coefficient. In an incompressible mixture, the Onsager coefficient takes the form $\Gamma \sim \phi_A \phi_B$ [38]. Inside an A domain, $\Gamma \sim \phi_B \sim \exp(-\chi N/2) \ll 1$ and, therefore, the thermodynamic driving force does not easily translate into a composition current. This observation constitutes a third reason why defect removal is protracted at large χN [39].

The main conclusion from our self-consistent field study [40] of defect removal is that (i) there exists an interval of incompatibility around $\chi N_* > \chi N_{ODT}$, in which microphase separation occurs but defects are not even metastable but spontaneously convert into defect-free structures and (ii) that the vicinity of the ODT additionally facilitates single-chain transport across internal interfaces, thereby accelerating the kinetics of defect removal. Since our numerical findings are related to physical mechanisms, we expect our conclusions to hold also for defects other than dislocation pairs. Rapid, defect-free DSA thus requires to match the chemistry of the copolymer material, χ, to the critical dimension, L_0, of the pattern, i.e., using high-χ materials to replicate structures with large L_0 by increasing the molecular weight, N, results in large χN and thus protracted defect removal.

This work was supported by the European Union FP7 under grant agreement 619793 CoLiSA.MMP (Computational Lithography for Directed Self-Assembly: Materials, Models, and Processes). WL thanks the National Natural Science Foundation of China (NSFC) (Grants Nos. 21322407 and 21174031) for additional financial support. Computing resources at SHARCNET were

kindly provided by R.A. Wickham, and additional resources were available at the HLRN (Hannover/Berlin) and the Jülich Supercomputing Center. JJdP and PFN are supported by the Department of Energy, Basic Energy Sciences, Materials Research and also acknowledge the Semiconductor Research Corporation (SRC).

[1] H. Hu, M. Gopinadham, C.O. Osuji, *Soft Matter*, **10**, 3867 (2014).
[2] M. Jacoby, *Chem. & Engineering News* **92**, 8 (2014).
[3] C.M. Bates, M.J. Maher, D.W. Janes, C.J. Ellison, and C.G.Willson, *Macromolecules*, **47**, 2 (2014).
[4] S.J. Jeong, J.Y. Kim, B.H. Kim, H.S. Moon, and S.O. Kim, *Mater. Today* **16**, 468 (2013).
[5] M. Luo and T.H. Epps III, *Macromolecules* **46**, 7567 (2013).
[6] K. Koo, H. Ahn, S.W. Kim, D.Y. Ryu, and T.P. Russell, *Soft Matter* **9**, 9059 (2013).
[7] J.K.W. Yang, J.S. Jung, J.B. Chang, R.A. Mickiewicz, A. Alexander-Katz, C.A. Ross, K.K. Berggren, *Nature Nanotech.* **5**, 256 (2010).
[8] K. Aissou, H.K. Choi, A. Nunns, I. Manners, C.A. Ross, *Nano Lett.* **13**, 835 (2013).
[9] R.A. Segalman, H. Yokoyama and E.J. Kramer, Adv. Materials **13**, 1152 (2001).
[10] J.Y. Cheng, A.M. Mayes, and C.A. Ross, Nature Mat. **3**, 823 (2004).
[11] R. A. Segalman, *Mat. Sci. & Engineering R-Rep.* **48**, 19 (2005).
[12] H. Takahashi, N. Laachi, K.T. Delaney, S.M. Hur, C.J. Weinheimer, D. Shykind, and G.H. Fredrickson, *Macromolecules* **45**, 6253 (2012).
[13] S.O. Kim, H.H. Solak, M.P. Stoykovich, N.J. Ferrier, J.J. de Pablo, and P.F. Nealey, *Nature* **424**, 411 (2003).
[14] M.P. Stoykovich, M. Müller, S.O. Kim, H.H. Solak, E.W. Edwards, J.J. de Pablo, P.F. Nealey, *Science* **308**, 1442 (2005).
[15] M.P. Stoykovich, H.M. Kang, P.F. Nealey, K.C. Daoulas, G.C. Liu, C.C. Liu, J.J. de Pablo, M. Müller, and P.F. Nealey, ACS Nano **1**, 168 (2007).
[16] R. Ruiz, H. Kang, F.A. Detcheverry, E. Dobisz, D.S. Kercher, T.R. Albrecht, J.J. de Pablo, and P.F. Nealey, *Science* **321**, 936 (2008).
[17] E.W. Edwards, M.P. Stoykovich, M. Müller, H.H. Solak, J.J. de Pablo, and P.F. Nealey, *J. Polym. Sci. B: Poly.. Phys.* **43**, 3444 (2005).
[18] U. Nagpal, M. Müller, P.F. Nealey, and J.J. de Pablo, *ACS Macro Lett.* **1**, 418 (2012).
[19] M. Müller and J.J. de Pablo, Annu. Rev. Mater. Sci. **43**, 1 (2013).
[20] M. Müller and F. Schmid, *Adv. Polym. Sci.* **185**, 1 (2005).
[21] Fredrickson, G. H., *The equilibrium theory of inhomogeneous polymers*, Oxford University Press, Oxford, UK (2006).
[22] X. Cheng, L. Lin, W. E, P. Zhang, and A.C. Shi, *Phys. Rev. Lett.* **104**, 148301 (2010).
[23] W. E, W. Ren, and E. Vanden-Eijnden, *J. Chem. Phys.* **126**, 164103 (2007).
[24] M. Müller and D.-W. Sun, *Phys. Rev. Lett.* **111**, 267801 (2013).
[25] C.-Z. Zhang and Z.-G. Wang, *Phys. Rev. E* **73**, 031804 (2006).
[26] M. Müller, *Phys. Rev. Lett.* **109**, 087801 (2012).
[27] S.P. Paradiso, K.T. Delaney, C.J. Gacía-Cervera, H.D. Ceniceros, and G.H. Fredrickson, *ACS Macro Letters* **3**, 16 (2014)
[28] A.A. Rudov, E.S. Patyukova, I.V. Neratova, P.G. Khalatur, D. Posselt, C.M. Papadakis, and I.I. Potemkin, *Macromolecules*, **46**, 5786 (2013).
[29] Y.S. Junk and C.A. Ross, *Nano Lett.* **7**, 2046 (2007).
[30] S.H. Kim, M.J. Misner, T. Xu, M. Kimura, and T.P. Russell, *Adv. Materials* **16**, 226 (2004).
[31] A.M. Welander, H. Kang, K.O. Stuen, H.H. Solak, M. Müller, J.J. de Pablo, and P.F. Nealey, *Macromolecules* **41**, 2759 (2008).
[32] Intriguingly, Zhang and Wang predict a glass-transition-like roughening of the free-energy landscape of block copolymers in a similar range of incompatibility [25].
[33] J.W. Cahn, *J. Chem. Phys.* **66**, 3667 (1977).
[34] Conceiving defect removal as wetting of the aligned grain on the guiding pattern ignores the finite, lateral extent of the defect and the concomitant additional contributions to the interface potential that arise from the distortion of the neighboring lamellae. Complementary, the specific, highly localized morphological change implicated in defect removal – breaking of the A connection – can also be regarded as wetting of the aligned B lamellae on the B-preferential stripe. In both cases, the (meta)stability is dictated by a balance between the difference of the surface free energy, $\gamma_{\rm sub}$, and the interface free energy of a grain boundary, $\gamma_{\rm gb}$, or an internal AB interface, γ_{AB}, respectively. Cahn's argument is applicable to both wetting phenomena.
[35] We have performed particle simulation of the evaporation mechanism ($\chi N = 30$,$D = 3L_0/4$), which followed the mechanism presented in Fig. 4. The protracted defect removal takes more than 500τ, where τ is the time for a copolymer to diffuse a distance $R_{\rm e0}$ at $\chi N = 0$. Defect-free assembly without barriers occurs within time τ [17].
[36] M. Müller and K.C. Daoulas, *Phys. Rev. Lett.* **107**, 227801 (2011).
[37] J. L. Barrat and G. H. Fredrickson, *Macromolecules* **24**, 6378 (1991).
[38] P. G. de Gennes, *J. Chem. Phys.* **72**, 4756 (1980).
[39] Additionally, the vicinity of the ODT reduces the free-energy barrier for breaking of the surrounding A domain in the vicinity of a dislocation. This morphological change directly connects the inner B domain of finite length, L, to the neighboring, infinitely extended B domain that can accommodate the excess B material and thereby circumvents the slow evaporation through the A domain.
[40] Fluctuations shift the ODT to larger incompatibility, $\chi N_{\rm ODT} \approx 10.5 + 41\bar{\mathcal{N}}^{-1/3}$ [G. H. Fredrickson and E. Helfand, *J. Chem. Phys.* **87**, 697 (1987)]. This shift chiefly stems from an inappropriate description of the disordered phase by the mean-field treatment [J. Glaser, *et al*, *Phys. Rev. Lett.* **113**, 068302 (2014)] implying that χN_* is much less affected by fluctuations than $\chi N_{\rm ODT}$. The condition, $\chi N_* > \chi N_{\rm ODT}$, results in a lower limit for $\bar{\mathcal{N}}$ and, thereby, for the smallest length scale achievable with high-χ materials. Using $\chi N_* = 18$, we obtain $\bar{\mathcal{N}} \gtrsim 160$, corresponding to $N \gtrsim 40$ monomeric repeat units of polystyrene or $L_0 \approx 1.6 R_{\rm e0} \gtrsim 7$nm.